Second-Order Predictive Direct Control of a Voltage Source Inverter Coupled to an LC Filter

Estanis Oyarbide [1], Josu Galarza [2], Sergio Aurtenechea [3], Miguel Ángel Rodríguez [2]

[1] Aragón Institute for Engineering Research (I3A), University of Zaragoza, María de Luna 1, 50018 Zaragoza, Spain
e-mail: eoyarbid@unizar.es
[2] Faculty of Engineering, University of Mondragon, Loramendi 4, Aptdo. 23, 20500 Mondragón, Spain
e-mail: jgalarza@eps.mondragon.edu
[3] Técnica de Automatismo y Medida, TEAM S.A., Parque Tecnológico- Edificio 108, E-48170 Zamudio (Bizkaia), Spain
e-mail: saurtenetxea@team.es

Abstract
The optimization of high power converters providing high-quality voltage levels and high- efficiency energy conversion leads to low switching frequencies and second-order LC filters with high resonant frequencies. Due to these narrow frequency ratios, classical control schemes comprising an inner current loop and an outer voltage loop are not feasible. The same applies to the single-loop dead-beat strategy or to the direct control technique, as their simple single-order predictive model does not offer the required level of accuracy. This article develops higher order prediction models and computes the prediction error for different frequency ratios and approximation orders. This analysis shows that in the case of an optimized industrial outage and sag compensator, a second-order prediction model provides the required accuracy; hence, the second-order predictive direct control is developed. This control drives both the inductor current and the capacitor voltage simultaneously, assures constant switching frequency, and results in robust and stable behaviour. Simulation and experimental results show the validity of the approach.

1. Introduction

During the last years, medium- and low-voltage grids have been interconnected to a large number of new active systems such as wind turbines, hydraulic generators, fuel cells, storage devices, power quality improvement units, and others. Almost all of these new installations are interconnected to the grid by means of a voltage source inverter (VSI) and a filter. Depending on the application, the VSI–filter system must offer high quality and fast driving capability of its output current (active filters, VAR compensator, etc.), voltage (dynamic voltage restorer, uninterrupted power system, etc.), or power (variable speed generators, fuel cells, etc.). This article focuses on systems delivering high quality voltage, that is, containing output filters of order two or higher (LC or LCL filter).

Typical industrial applications require low-cost and efficient systems; therefore, some constraints concerning the reactive elements of the filter and the switching frequency must be considered. When high efficiency is desired (particularly in high power systems), switching losses must be minimized, that is, low switching frequency is preferably used [1]–[7]. On the other hand, though a high LC value improves the output voltage quality, it increases the filter cost, the VSI must be oversized in order to keep the same nominal output rating, and the overall dynamic is penalized. Because of this, the minimum LC value that complies with connection regulations in terms of harmonics and THD must be selected [8], [9].

In the frame of high-power systems with optimized reactive elements, the high resonance frequency of the filter (f_0) combined with the low switching frequency of the VSI (f_{sw}) leads to narrow frequency ratios $m = f_{sw}/f_0 < 5$. This is the case of the high power converters of $(3 < m < 4.2)$ [1], ($m = 2.7$) [2], and ($m = 3.9$) [9]. Most of the works related to control tasks consider high $m = f_{sw}/f_0$ ratios (above 10), which make it possible to implant well-known control strategies [8]–[11]. This is the case of the multiloop, dead-beat control scheme, with an inner current loop and an outer and slower voltage loop [9],[10], or the single loop dead-beat case [11]. The same applies for direct control schemes, where the first-order Taylor approximation offers an accurate prediction of the evolution of filter variables.

However, when low $m = f_{sw}/f_0$ ratios are considered, it is not possible to decouple the inductor current dynamics from that of the capacitor voltage; hence, high dynamic multiloop schemes are not feasible [9]. Similarly, in the case of direct control schemes, the first-order Taylor approximation does not reflect the evolution of the state with the desired level of accuracy, as will be shown later. Generally, the control of these types of systems is achieved by conservative strategies and includes a filter stabilization facility, for example, a damping resistor (penalizing the overall efficiency) [5],[12], or any active stabilization strategy superposed to the control scheme [2]

Therefore, when optimal device ratings with low $m = f_{sw}/f_0$ ratios are applied and high dynamic is desired, the simplified prediction model must be built around a higher-degree Taylor approximation.

In this framework it could be of interest to develop a second-order predictive direct control (SO-PDC) of a VSI coupled to an LC filter. Predictive and direct controls are usually employed in systems with single inductive filters [3],[6], [13],[17] but there are no references concerning predictive direct control of both the inductor current and the capacitor voltage. This article explains first the fundamentals of predictive direct control of a three-level VSI coupled to an LC filter. Next, the accuracy of prediction is analyzed, concluding that in the application example, a second-order Taylor approximation is needed. Then the second-order predictive direct control problem is stated and solved. Finally, some simulation and experimental results validate the proposed approach.

2. Fundamentals of Predictive Direct Control

A typical example of a VSI coupled to an LC filter is depicted in Fig. 1a. It represents a one-phase three-level dynamic voltage restorer (DVR), which can be considered as part of a four-wire three-phase system [8]. The DVR must add the required series voltage in order to compensate sags or short outages of the power source (v_s) in such a way that nominal output load voltage is assured (v_L). Therefore, the goal of any DVR control is to drive the output capacitor voltage (v_c) as fast as possible close to the reference value, minimizing the tracking error.

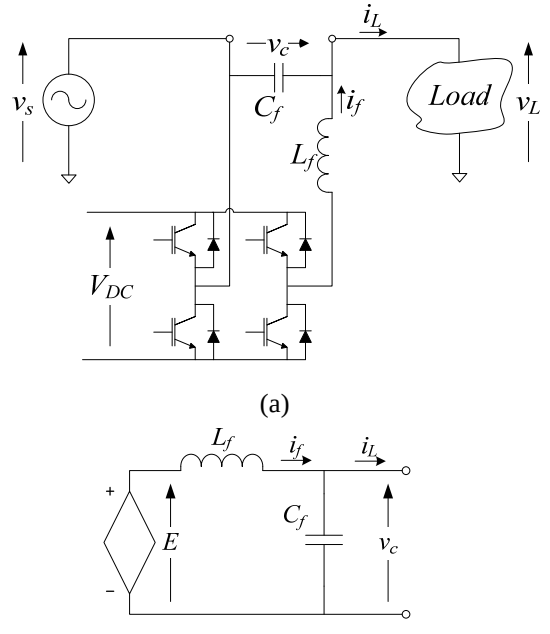

Fig. 1 *Three-level VSI coupled to an LC filter: (a) one phase DVR, (b) equivalent circuit.*

Fig. 1b. shows the equivalent circuit of the system of Fig. 1a. The VSI can apply one of the three available voltage levels $E \in \{0, V_{DC}, -V_{DC}\}$ and the line current is considered as a perturbation.

2.1 Modulation cycle definition

Direct predictive control is based on the so-called modulation cycle. A modulation cycle can be defined as the concatenated application of the three available voltage levels.

$$E_1, E_2, E_3 \in \{0, V_{DC}, -V_{DC}\},$$
$$E_1 \neq E_2, \quad E_2 \neq E_3, \quad E_1 \neq E_3$$

The control technique must select the appropriate sequence of application of voltage levels $\{E_1, E_2, E_3\}$ and the time of application of each level $\{t_1, t_2, t_3\}$, in such a way that constant predefined switching frequency is assured, that is,

$$t_1 + t_2 + t_3 = T_{sw} \tag{1}$$

Fig. 2a shows an example of a modulation cycle using the sequence of voltage levels $\{E_1, E_2, E_3\} = \{0, V_{DC}, -V_{DC}\}$.

It has to be noted that the main control idea behind this strategy has been explored earlier in other works [6],[17], but they dealt with simple inductive filters related to first-order Taylor approximation.

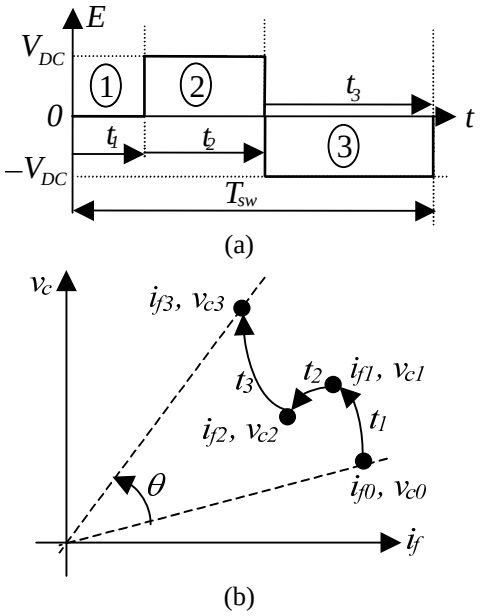

Fig. 2 *(a) Modulation cycle example. (b) State evolution along a modulation cycle.*

2.2 Formulation of the Predictive Direct Control Problem

When a modulation cycle is applied the state evolves along three concatenated continuous trajectories (see Fig. 2b). Table 1 summarizes the set of variables related to each trajectory.

Table 1: Concatenated segments

Segment	*Application time*	*Initial state*	*Final state*
1	t_1	i_{f0}, v_{c0}	i_{f1}, v_{c1}
2	t_2	i_{f1}, v_{c1}	i_{f2}, v_{c2}
3	t_3	i_{f2}, v_{c2}	i_{f3}, v_{c3}

The state and evolution of the variables of the LC filter of Fig. 1b. are exclusively driven by the output voltage of the inverter, E, and by the line-current i_L. If the line-fundamental frequency is several times lower than the switching frequency, it can be supposed that the line-current i_L stays at a quasi constant value i_{L0} along the switching period T_{sw}. As the line-voltage does not affect the evolution of the variables of the LC filter, it is not necessary to consider any complementary supposition related to this variable. Under these assumptions, the state evolution along any segment of the modulation sequence is accurately reflected by Eqs (2) and (3):

$$\begin{aligned} i_{fi} &= E_i C_f \omega_o \sin(\omega_o t_i) + i_{L0}(1-\cos(\omega_o t_i)) \\ &\quad - v_{c(i-1)} C_f \omega_o \sin(\omega_o t_i) + i_{f(i-1)} \cos(\omega_o t_i) \end{aligned} \tag{2}$$

$$\begin{aligned} v_{ci} &= E_i(1-\cos(\omega_o t_i)) - i_{L0} L_f \omega_o \sin(\omega_o t_i) \\ &\quad + v_{c(i-1)} \cos(\omega_o t_i) + i_{f(i-1)} L_f \omega_o \sin(\omega_o t_i) \end{aligned} \tag{3}$$

with $i \in \{1,2,3\}$ the segment index and

$$\omega_o = \frac{1}{\sqrt{L_f C_f}} \tag{4}$$

the resonant frequency of the filter.

The predictive direct control problem is formulated as follows: knowing the initial state of the system (i_{f0}, v_{c0}), it is necessary to select the sequence of voltage levels $\{E_1, E_2, E_3\}$ and their application times $\{t_1, t_2, t_3\}$ in such a way that the desired final state (i_{f3}, v_{c3}) is reached during the constant switching period T_{sw} (1).

There are three segments and two equations per segment, which leads to six equations defining the trajectories. Considering the additional constant switching restriction (1), a set of seven equations and seven variables are obtained; hence, the exact analytical solution shown in Eq. (5) is forecasted. In the case of a mismatch between the number of variables and equations, an approximate solution using the least square optimization is explored [18].

$$t_i = f_i(T_{sw}, i_{f0}, v_{c0}, i_{f3}, v_{c3}, i_{L0}, E_1, E_2, E_3) \tag{5}$$

The presence of trigonometric functions on the control problem makes it difficult to obtain this analytical solution. In order to overcome this problem, simpler approximate equations must be used in the prediction of the state evolution.

The DVR application provides only the desired final capacitor voltage, $v_{c3;}$ hence, it is necessary to derive the desired final inductor current, i_{f3}. A transient can be considered as the evolution of the system from an initial steady-state situation to a new steady-state operation point. Therefore, a simple steady-state phasor-based analysis will provide the required final inductor current, i_{f3}. The DVR control algorithm provides the phasor of the desired capacitor's voltage, $\overrightarrow{V_c}$ and due to an appropriate PLL it is easy to get the line-current phasor $\overrightarrow{I_L}$. Using simple circuit relations it is possible to compute the inductor's current phasor (6).

$$\overrightarrow{I_f} = \frac{\overrightarrow{V_C}}{\overrightarrow{X_C}} + \overrightarrow{I_L} \tag{6}$$

As the state evolves during T_{sw} seconds, the desired final instantaneous variables are computed as the projection of these phasors along T_{sw}.

$$\begin{aligned} v_{c3} &= V_{c\max} \cos(\omega(t+T_{sw}) - \theta_c) \\ i_{f3} &= I_{f\max} \cos(\omega(t+T_{sw}) - \theta_i) \end{aligned} \tag{7}$$

If the switching period is much smaller than the line-period, T_{sw} can be neglected in (7).

3. Accuracy of the approximate prediction

The sine and cosine functions of trajectory description (2)–(3) can be replaced by their equivalent Taylor series:

$$\sin(\omega_o t) \approx \omega_o t - \frac{(\omega_o t)^3}{3!} + \frac{(\omega_o t)^5}{5!} - \dots \tag{8}$$

$$\cos(\omega_o t) = 1 - \frac{(\omega_o t)^2}{2!} + \frac{(\omega_o t)^4}{4!} \dots \tag{9}$$

The maximum error of the Taylor development of the sine or cosine function is bounded by the first noncomputed term, which changes each odd or even degree. Assuming that the state evolves during $t_i = T_{sw}/2$, Eqs (10) and (11) give the maximum error related to an even (odd) order n of approximation (derivation in Appendix 10.1).

$$\begin{bmatrix} |\varepsilon_{if}| \\ |\varepsilon_{vc}| \end{bmatrix} < \frac{\pi^{n+1}}{m^{n+1}(n+1)!} \begin{bmatrix} \frac{\pi}{m(n+2)} & \sqrt{\frac{C}{L}} \\ \sqrt{\frac{L}{C}} & \frac{\pi}{m(n+2)} \end{bmatrix} \begin{bmatrix} |\Delta i| \\ |\Delta v| \end{bmatrix} \tag{10}$$

$$\begin{bmatrix} |\varepsilon_{if}| \\ |\varepsilon_{vc}| \end{bmatrix} < \frac{\pi^{n+1}}{m^{n+1}(n+1)!} \begin{bmatrix} 1 & \sqrt{\frac{C}{L}} \frac{\pi}{m(n+2)} \\ \sqrt{\frac{L}{C}} \frac{\pi}{m(n+2)} & 1 \end{bmatrix} \begin{bmatrix} |\Delta i| \\ |\Delta v| \end{bmatrix} \tag{11}$$

with

$$m = \frac{f_{sw}}{f_0} \tag{12}$$

and,

$$f_0 = \frac{\omega_0}{2\pi} \qquad \Delta i = i_{f(i-1)} - i_{L0}, \qquad \Delta v = v_{c(i-1)} - E_i$$

Thus the per-unit errors are computed as:

$$\varepsilon_{ifpu} = \frac{|\varepsilon_{if}|}{i_{L\max}}, \qquad \varepsilon_{vcpu} = \frac{|\varepsilon_{vc}|}{v_{L\max}} \tag{13}$$

Therefore, the per-unit maximum normalized error of state approximation is:

$$\varepsilon_{pu} = \sqrt{\varepsilon_{ifpu}^2 + \varepsilon_{vcpu}^2} \tag{14}$$

Fig. 3 shows an example of the per-unit maximum normalized error (%) along different approximation orders (n) and frequency ratios (m). Parameters of an industrial low-voltage high-power DVR [9] have been employed, with $L_f = 39\mu H$, $C_f = 1100\mu F$, $V_{DC} = 550V$, $v_{L\max} = v_{c\max} = \sqrt{2}\cdot 230V$, and $i_{L\max} = 3000A$. As it can be observed, for high $m = f_{sw}/f_0$ ratios a first-order Taylor development offers a good accuracy level ($\varepsilon_{pu} < 25\%$) and it can be used in control design tasks. In the case of low m values ($2<m<5$) second- or third-order development must be employed in order to get the same level of accuracy.

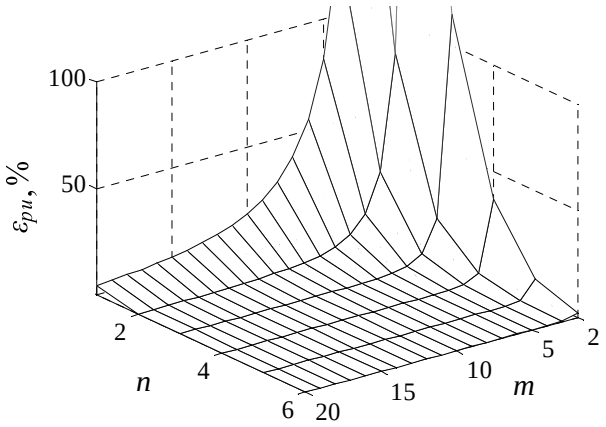

Fig. 3 *Normalized maximum error of state approximation depending on the development order n and the frequency ratio* $m = f_{sw}/f_0$.

In the numerical example of this article $f_0 = 768Hz$ and $f_{sw} = 3000Hz$; hence, a challenging low frequency ratio of $m = 3.9$ is obtained. Fig. 3 shows that for a second-order development the maximum prediction error is approximately 30%, which can be considered as acceptable. Although the third-order approximation improves this accuracy, the control problem is more complex. Hence, the second-order is finally preferred, leading to the *Second-Order* Predictive Direct Control.

Uncertainty on the estimation of C_f and L_f can also be a source of error in the prediction of the state evolution. Taking $\hat{C}_f$ and $\hat{L}_f$ as the estimated values of C_f and L_f, considering $\hat{i}_f$ and $\hat{v}_c$ the estimated evolutions of i_f and v_c, and using Eqs (2) and (3), it is possible to compute the prediction errors as follows:

$$\varepsilon_{if} = \hat{i}_f(t) - i_f(t) = (E - v_c(0))\omega_o \sin\left(\frac{\omega_o T_{sw}}{2}\right)\left(\hat{C}_f - C_f\right) - \Delta v \omega_o \sin\left(\frac{\omega_o T_{sw}}{2}\right) C_f \delta_C \tag{15}$$

$$\varepsilon_{vc} = \hat{v}_c(t) - v_c(t) = \left(i_f(0) - i_{L0}\right)\omega_o \sin\left(\frac{\omega_o T_{sw}}{2}\right)\left(\hat{L}_f - L_f\right) = \Delta i \omega_o \sin\left(\frac{\omega_o T_{sw}}{2}\right) L_f \delta_L \tag{16}$$

with $\delta_C = \left(\hat{C}_f - C_f\right)/C_f$ and $\delta_L = \left(\hat{L}_f - L_f\right)/L_f$, the per-unit difference between the estimated and the actual parameter values. The normalized prediction error can be derived from Eqs (13), (15), and (16). In the case of the industrial low-voltage high-power DVR example of the earlier paragraph [9], an uncertainty level of 22% on the capacitor's value leads to a prediction error of approximately 25%, which can be considered acceptable. In the case of the inductor value, an uncertainty level of 10% results in the same prediction error. Experimental uncertainty levels of capacitors and inductors are below these values; hence, a robust behaviour of the SO-PDC against uncertainty on the filter's parameters is expected.

4. Second-order predictive direct control

The predictive direct control must find out a solution of Type (5) using the trajectory description (2)–(3) under the constant switching frequency constraint (1). As explained earlier, the second-order Taylor's development offers a compromise between accuracy and ease of implementation; hence, Eqs (2) and (3) are replaced by their approximate equivalents (17),(18).

$$i_{fi} \approx \frac{E_i - v_{c(i-1)}}{L_f} t_i + i_{f(i-1)}\left(1 - \frac{\omega_o^2 t_i^2}{2}\right) + i_{L0}\frac{\omega_o^2 t_i^2}{2} \tag{17}$$

$$v_{ci} \approx v_{c(i-1)}\left(1 - \frac{\omega_o^2 t_i^2}{2}\right) + E_i \frac{\omega_o^2 t_i^2}{2} + \left(i_{f(i-1)} - i_{L0}\right) L_f \omega_o^2 t_i \tag{18}$$

Solving the set of seven equations and seven variables and retaining only the terms of order two or lower, the solution to the control problem (the application times) is derived (19)–(21) (see Appendix 10.2 for the complete derivation and the equivalences of coefficients).

$$t_2 = \frac{2\sqrt{b_0}}{a_0 \omega_0} \tag{19}$$

$$t_1 = \frac{1}{c_0}\left(c_1 t_2 + c_2 i_{f3} + (c_3 - c_2) i_{f0} + c_4 v_{c0} - c_3 i_{L0} - c_5\right) \tag{20}$$

$$t_3 = T_{sw} - t_1 - t_2 \tag{21}$$

The selection of the appropriate voltage sequence remains as a problem to be solved. Table 2 shows all the possible

voltage sequences. The only mandatory restriction related to voltage sequence selection is that it must provide non-negative solutions of Eqs (19)–(21). There are two subsets of sequences, $S_A = \{S_1, S_3, S_5\}$ and $S_B = \{S_2, S_4, S_6\}$, which lead, alternatively, to nonnegative solutions, that is, if any of the sequences of subset S_A does not provide a coherent solution, it is provided by any of the sequences of the subset S_B, and vice versa. The subset S_A is made up of sequences applying the positive voltage level before the negative one, and the subset S_B collects the other three sequences. Generally, each one of the subsets is applied during a half of the line-fundamental period, but the commutation from one subset to the other depends on the line current, capacitor voltage, and inductor current.

Table 2: Possible sequences

Sequence	E_1	E_2	E_3
S_1	0	V_{DC}	$-V_{DC}$
S_2	0	$-V_{DC}$	V_{DC}
S_3	V_{DC}	$-V_{DC}$	0
S_4	$-V_{DC}$	V_{DC}	0
S_5	V_{DC}	0	$-V_{DC}$
S_6	$-V_{DC}$	0	V_{DC}

In order to get a coherent solution of Eq. (19), both b_0 and a_0 must be positive in such a way that real (nonimaginary) and positive application time t_2 is obtained. Considering the example of the two first sequences S_1 and S_2, that is, $E_1 = 0V$ and $E_2, E_3 \in \{V_{DC}, -V_{DC}\}$, and using the equivalences of Appendix 10.2, next values are obtained:

$$a_0 = 8{E_2}^2 \tag{22}$$

$$b_0 = g(i_{f0}, i_{f3}, i_{L0}, v_{c0}) + 2{E_2}^2 E_3 \left(8{\omega_0}^2 T_{sw} L_f (i_{f0} - i_{L0}) - 8(v_{c3} - v_{c0}) - 4{\omega_0}^2 {T_{sw}}^2 v_{c0}\right) \tag{23}$$

with

$$g(i_{f0}, i_{f3}, i_{L0}, v_{c0}) = -2{E_2}^2 \left\{ \begin{array}{l} 4{\omega_0}^2 {L_f}^2 {i_{f3}}^2 + 8{\omega_0}^2 {L_f}^2 T_{sw} v_{c0} i_{f3} + \\ + \left(4{\omega_0}^4 {L_f}^2 {T_{sw}}^2 - 8{\omega_0}^2 {L_f}^2\right) i_{f0} i_{f3} + \\ + 4{\omega_0}^4 {L_f}^2 {T_{sw}}^2 i_p i_{f3} - 4{\omega_0}^2 {T_{sw}}^2 {v_{c0}}^2 - \\ - \left(-8{\omega_0}^2 L_f T_{sw} + 4{\omega_0}^4 L_f {T_{sw}}^3\right) v_{c0} i_{f0} + \\ + 4{\omega_0}^4 L_f {T_{sw}}^3 i_{L0} v_{c0} - \\ - \left(\begin{array}{l} {\omega_0}^6 L_f {T_{sw}}^4 \\ - 4{\omega_0}^4 {L_f}^2 {T_{sw}}^2 + 4{\omega_0}^4 {L_f}^2 \end{array} \right) {i_{f0}}^2 - \\ - \left(-2{\omega_0}^6 {L_f}^2 {T_{sw}}^4 + 4{\omega_0}^4 {L_f}^2 {T_{sw}}^2\right) i_{L0} i_{f0} - \\ - {\omega_0}^6 {L_f}^2 {T_{sw}}^4 i_{L0} \end{array} \right\} \tag{24}$$

As a_0 is always positive, a coherent solution will be assured if b_0 is positive. For a given initial state and current reference values $g(i_{f0}, i_{f3}, i_{L0}, v_{c0})$ remains constant; hence, the sign of b_0 will only change if the second term of (23) changes. As ${E_2}^2$ is always positive and constant, the sign of b_0 can be computed as follows:

$$sign(b_0) = sign\left\{ \frac{g(i_{f0}, i_{f3}, i_{L0}, v_{c0})}{2{E_2}^2} + E_3 \left(8{\omega_0}^2 T_{sw} L_f (i_{f0} - i_{L0}) - 8(v_{c3} - v_{c0}) - 4{\omega_0}^2 {T_{sw}}^2 v_{c0}\right) \right\} \tag{25}$$

If (25) is divided by $8T_{sw}$, which keeps the sign, and combining (4) and (12) with (25), a more useful expression is obtained:

$$\begin{aligned} sign(b_0) &= sign\left\{ \frac{g(i_{f0}, i_{f3}, i_{L0}, v_{c0})}{16 T_{sw} {E_2}^2} + E_3 \left(\frac{1}{C_f}(i_{f0} - i_{L0}) - \frac{(v_{c3} - v_{c0})}{T_{sw}} - \frac{1}{2} \frac{2\pi}{2\pi / T_{sw}} {\omega_0}^2 v_{c0} \right) \right\} = \\ &= sign\left\{ \frac{g(i_{f0}, i_{f3}, i_{L0}, v_{c0})}{16 T_{sw} {E_2}^2} + E_3 \left(\left.\frac{dv_c}{dt}\right|_0 - \left.\frac{dv_c}{dt}\right|_{ref} - \frac{\pi}{m} \omega_0 v_{c0} \right) \right\} \end{aligned} \tag{26}$$

with $\left.\frac{dv_c}{dt}\right|_0$ the initial time-derivative of v_c and $\left.\frac{dv_c}{dt}\right|_{ref}$ the desired average time-derivative along T_{sw}. In steady-state operation, these two derivatives are practically equivalent; hence, the next approximate equivalent of (26) can be obtained:

$$sign(b_0) \approx sign\left\{ \frac{g(i_{f0}, i_{f3}, i_{L0}, v_{c0})}{16 T_{sw} {E_2}^2} - \frac{\pi}{m} \omega_0 E_3 v_{c0} \right\} \tag{27}$$

In the case of large and positive v_{c0} values, the control problem will lead to a coherent solution only if $E_3 = -V_{DC}$, i.e., if the first sequence (S_1) is chosen. In the case of large and negative v_{c0} values, the second sequence with $E_3 = V_{DC}$ must be chosen (S_2). Similar analysis leads to equivalent conclusions if sequences S_3 and S_4 or S_5 and S_6 are used. These results match with the observed behaviour, as shown in Section 5.

This article exploits a simple voltage sequence selection strategy: a given subset of sequences is used until it does not provide a coherent set of application times, and when that happens, the control simply commutes to the other subset of voltage sequences, leading to feasible positive application times.

Once the appropriate subset of sequences is identified, it is necessary to know which one of the three possible sequences must be employed. This selection could be made according to any optimization criteria, such as the level of injected harmonics, efficiency constraints, or others. This topic is still under research and the work presented here is based on a simple sequence selection

strategy that exploits only two voltage sequences, that is, $S_1 \in S_A$ and $S_2 \in S_B$. The control must simply change from one possible sequence to another (S_1 or S_2) each time the application time solution becomes incoherent.

5. Simulation results

The parameters of the simulated system are the same as the industrial low-voltage high-power DVR of Section 3 [9] and simulations have been carried out under the MATLAB/SIMULINK environment. As pointed out earlier, the parameters of this DVR-example lead to a frequency ratio of m=3.9 which makes it difficult to exploit the first-order model in control synthesis tasks. This difficulty emerges immediately when a standard control technique such as the multiloop dead-beat control approach is tried. The multiloop dead-beat control is built around an inner inductor's current control loop and an outer capacitor's voltage loop and has been successfully employed in systems with high m ratios (see [8]–[11] and [19]–[22]). Among the different possible ways of developing the dead-beat control, the RST structure [21],[22] and the "difference equations" approach [19],[20] can be used. Following the RST synthesis procedure explored in [21] and [22], the inner-current control-loop has been designed, leading to the zero-pole map of Fig.4. This figure shows the poles for three different switching frequencies: f_{sw}=10 KHz (m=13), f_{sw}=5 KHz (m=6.5), and f_{sw}=3 KHz (m=3.9). The last case is the application example of this paper. As it can be observed Fig. 4, when the frequency ratio decreases, the poles approach the stability border defined by the unit circle. When the frequency ratio falls down to m=3.9, two unstable poles out of the unity circle appear. Therefore, it is not possible to exploit the first-order model-based dead-beat control in the case of this DVR example. This result launched the research activity that culminated in the proposal of this article, the SO-PDC.

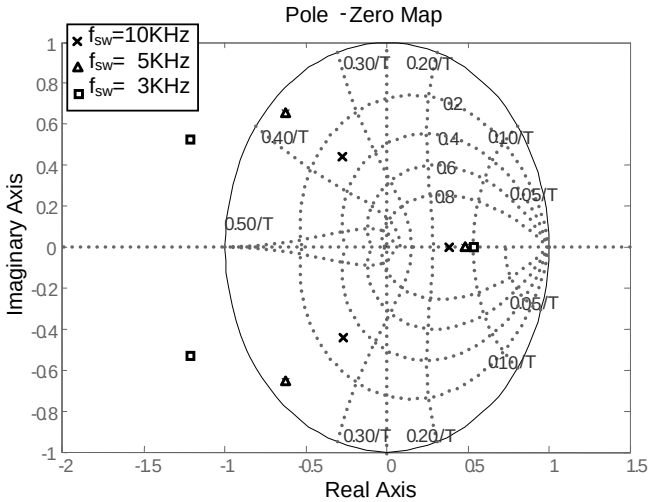

Fig. 4 *Pole-zero map of the dead-beat control of the inner current loop. Poles related to three possible switching frequencies are shown.*

In the frame of SO-PDC simulations, both the reference tracking behaviour and the regulation capability have been analyzed. In the first case, Fig. 5, a reference voltage-step has been applied to the filter capacitor. As observed, the capacitor voltage reaches the desired new value in just one switching sequence, and the resulting voltage and current values are always kept close to the reference. Fig. 6 shows the state-space trajectory derived from a start-up transient (from [v_{c0}=0pu, i_{f0}=0pu] to [v_{c3}=0.9pu, i_{f3}=0pu]), followed by a half-cycle steady operation, a second transient (depicted in Fig. 5), and a final half-cycle steady operation.

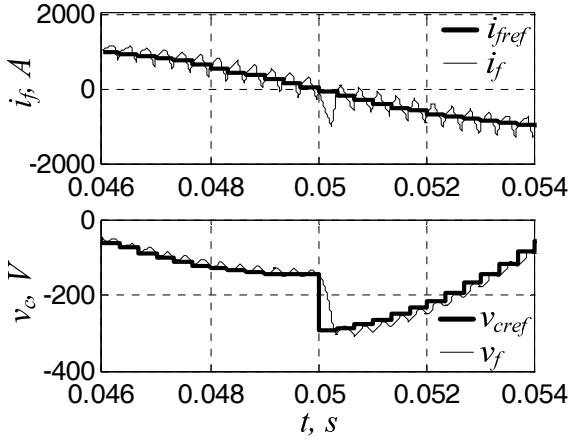

Fig. 5 *Voltage step, simulation.*

The regulation capability of the DVR is analyzed by a load current step, which implies a current step on the filter inductor, see Fig. 7a. The current reaches the required value in only one switching sequence, and the same stable and well-behaved transient as in the earlier case is observed.

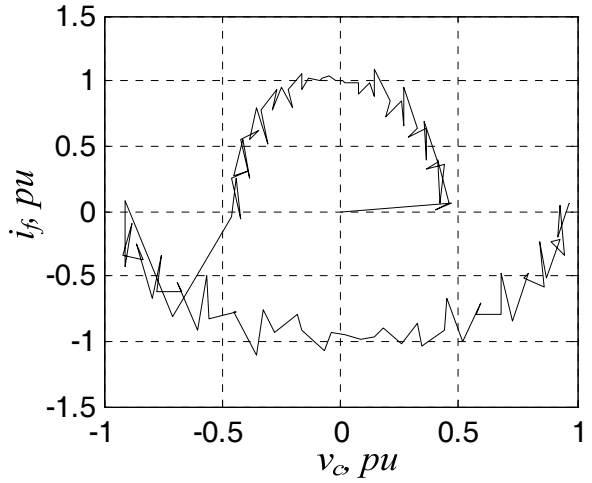

Fig. 6 *State-space trajectory comprising starting transient and voltage step, simulation.*

Fig. 7b. shows the voltage at the output of the VSI together with the sequence number employed in each modulation cycle. As observed, the selected sequence follows, in a general way, the law that has been predicted in Section 4 (S_1 for large positive v_c values and S_2 for large negative v_c values).

Simulation results are quite satisfactory, and considering that it is the simplest SO-PDC strategy and that

several improvements would be still possible, it seems to be a promising approach.

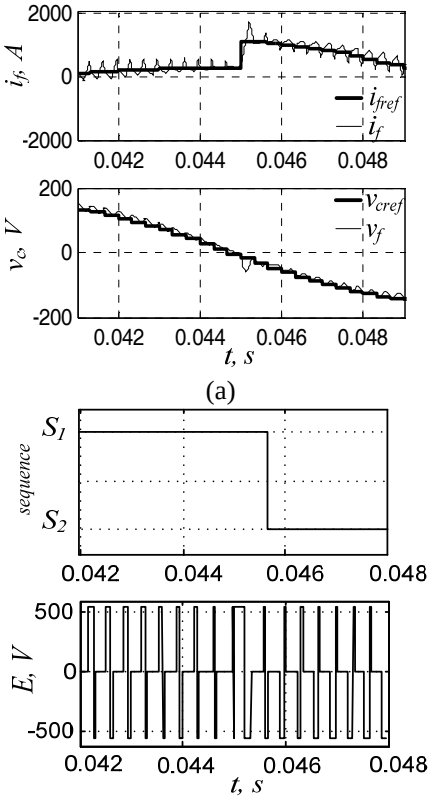

Fig. 7 *Current step caused by a load variation, simulation: (a) current–voltage response, (b) selected sequence and applied voltages.*

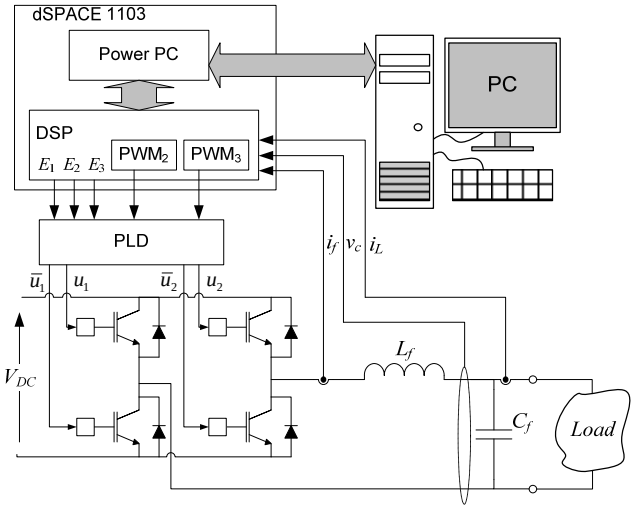

Fig. 8 *Experimental setup*

6. Experimental results

In order to validate the proposed control algorithm, experimental tests have been carried out at the Power Electronics Laboratory of the University of Mondragon. The control algorithm has been implanted on a real-time dSPACE 1103 platform. This platform offers predefined standard SVM and PWM blocks. Therefore, several adaptations have to be done in order to implement the SO-PDC. The SO-PDC comprises: (a) the measurement of the state-variables at the beginning of the switching period, (b) the generation of the current-voltage reference, and (c) the derivation of the appropriate application times. The execution time of the SO-PDC algorithm takes $t_D = 110\mu\text{sec}$, which is the 10% of the switching period $T_{sw} = 1/975 = 1025\mu\text{sec}$.

An overview of the experimental platform is given in Fig. 8 and the simplified control block diagram is depicted in Fig. 9. Fig. 10 shows the timing diagram related to the generation of application times from t_k to t_{k+1}. Experimental variables must be sampled close to t_k, observing the time delay t_D required for control tasks. This can be easily achieved by launching a timing equal to T_{sw}-t_D at t_{k-1}. This timing is accurately generated by a first PWM1 related to an interruption that starts the execution of the SO-PDC algorithm.

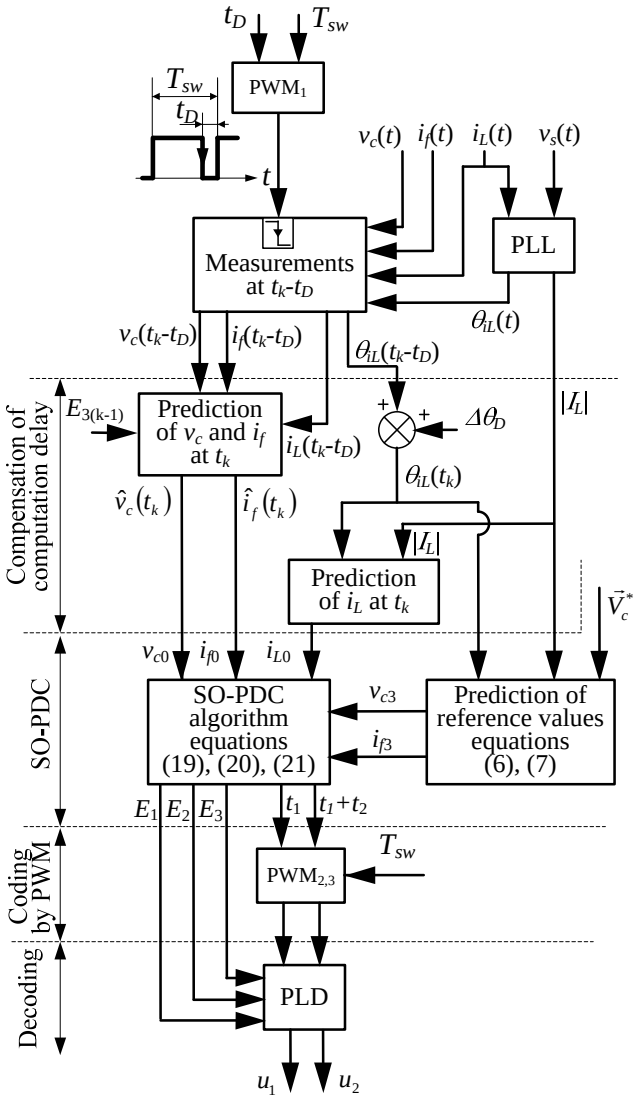

Fig. 9 *Control block diagram*

Variables are measured $t_D = 110\mu\text{sec}$ before the beginning of the cycle; hence, a prediction of their evolution must be carried out in order to estimate the initial state at t_k. As t_D is much smaller than T_{sw}, a simple first-order model is used for predicting the state evolution during the execution of

SO-PDC tasks. Once the SO-PDC has been executed and the application times from t_k to t_{k+1} are available at t_k, they are coded through two additional PWM blocks (PWM2 and PWM3). The outputs of these PWM signals are then decoded by conventional logic circuits and applied to the switching drivers.

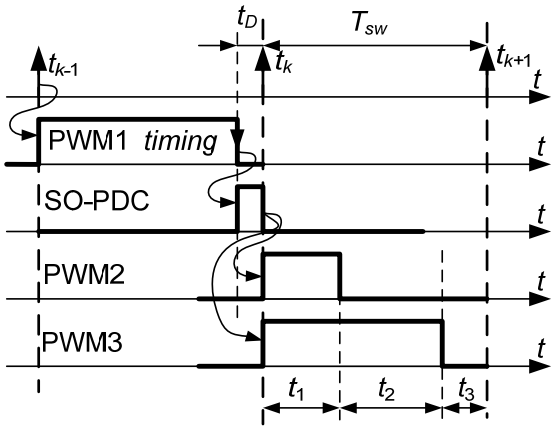

Fig. 10 *Experimental timing diagram*

Table 3 summarizes the main parameters of both the industrial and the experimental DVR with several related important ratios. The experimental laboratory setup is shared with other research activities, so it does not have exactly the same parameters of the industrial DVR. Any way, it has been adapted in order to get an experimental filter with the same frequency ratio (m=3.9) of the industrial DVR. Therefore, the laboratory setup requires the same second-order development. Moreover, the experimental platform shows lower f_{sw}/f_1 and f_0/f_1 ratios.

Table 3: Converter parameters

Variable	1.6 MVA DVR	Experimental DVR
L_f	$39\mu H$	$52mH$
C_f	$1100\mu F$	$8\mu F$
V_{DC}	$550V$	$100V$
f_1	$50Hz$	$50Hz$
f_0	$768Hz$	$247Hz$
f_{sw}	$3000Hz$	$975Hz$
$m = f_{sw}/f_0$	3.9	3.9
f_{sw}/f_1	60	19.5
f_0/f_1	15.36	5

Fig. 11 shows the experimental steady-state behaviour of both the inductor's current and the capacitor's voltage. Although the resonance frequency is very close to the switching frequency, SO-PDC results in a very stable behaviour and keeps the two variables close to the reference values. Fig. 12 depicts the experimental transient behaviour of the SO-PDC when a reference step is applied. The reference tracking capability is excellent and both variables reach the new reference values in just one switching sequence. Several different scenarios (different switching frequencies, filter's parameters, etc.) have been experimentally tested, and the SO-PDC has worked properly in all cases, showing a high level of robustness.

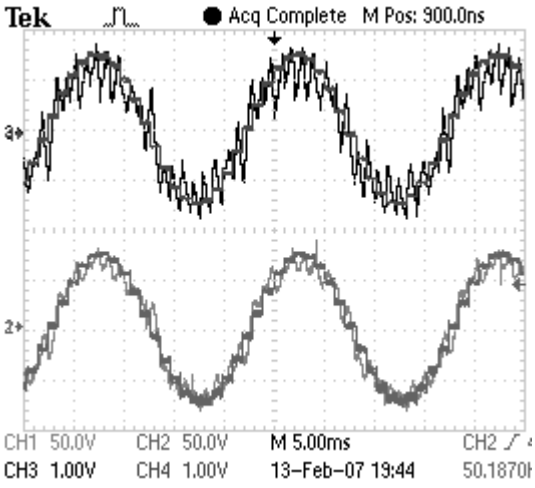

Fig. 11 *Experimental steady-state evolution of current (up, 1 A/div) and voltage (down, 50 V/div) with associated reference.*

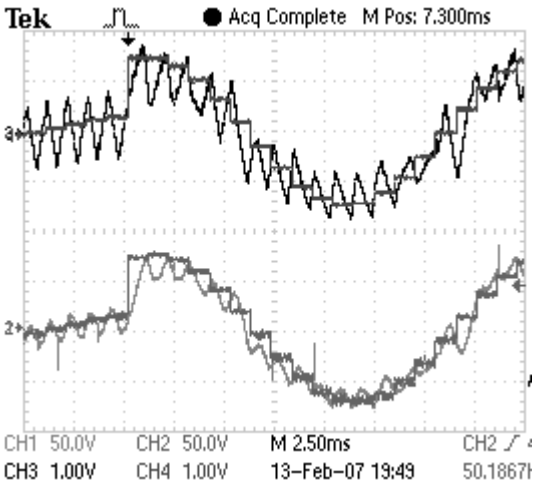

Fig. 12 *Experimental response of current (up, 1 A/div) and voltage (down, 50 V/div) during a reference-step.*

7. Conclusions

In the frame of high-power electronic converters, low switching frequency together with optimized LC filters leads to poor switching frequency–resonant frequency ratios, in such a way that common predictive models based on the first-order Taylor's development are not precise enough. These low ratios make the application of habitual direct control techniques difficult. This problem can be solved by increasing the approximation order up to the required level of accuracy. Taking a high power DVR as the application example, a second-order model has been developed, leading to excellent transient and steady-state behaviours. Experimental tests have validated the proposed approach. One of the main characteristics of this control scheme is the dual tracking capability, driving both the capacitor's voltage and inductor's current simultaneously. Because of the dual tracking capability of the SO-PDC, the maximum available system's dynamic is exploited and

faster transient response and stable behaviour for systems with weak LC filters are provided. The dual tracking capability also provides an inherent stabilizing feature; hence, no additional damping resistors or superposed stabilizing algorithms are needed. The proposed second-order predictive direct control has shown a high level of robustness in experimental environment, and could be an alternative for high-power electronic converters.

In the case of three-wire three-phase converters, preliminary numerical results on the accuracy of the Taylor's approximation reflect the need for the same second-order model. Research on the generalization of the SO-PDC approach to the three-wire three-phase case will be addressed in the future.

8. Acknowledgements

This work has been supported by the programs ENE2005-09218-C02-01/02 and ENE2006-15339-C02-01/02 from MCYT DGI/FEDER.

9. References

[1]Bernet, S.: 'State of the Art and Developments of Medium Voltage Converters-An Overview', *International Conference on Power Electronics and Intelligent Control for Energy Conservation, PELINCEC,* Warsaw, Poland 2005, Paper ID: 254

[2]Bernet, S.: 'Recent Developments of High Power Converters for Industry and Traction Applications', *IEEE Transactions on Power Electronics,* 2000, vol. 15, no. 6, pp. 1102-1117

[3]Holtz, J.: 'Pulsewidth Modulation for Electronic Power Conversion', *Proceedings of the IEEE,* 1994, vol. 82, no. 8, pp. 1194-1214

[4]Holtz, J. and Beyer, B.: 'The Trajectory Tracking Approach-A New Method for Minimum Distorsion PWM in Dynamic High-Power Drives', *IEEE Transactions on Industry Applications,* 1994, vol. 30, no. 4, pp. 1048-1057

[5]Allmeling, J. and Stemmler, H.: 'A fast current control technique for active filters with low switching frequency', *IEEE Annual Conference of the Industrial Electronics Society, IECON,* Denver, USA, 2001, vol. 2, pp. 1125-1131

[6]Sariñana, A., Guffon, S., Bornard, G., and Bacha, S.: 'A novel fixed switching frequency controller of a three-phase voltage source inverter', *European Power Electronics Conference, EPE,* Lausanne, Switzerland 1999, CD-ROM

[7]Joós, G., Huang, X., and Ooi, B.-T.: 'Direct-coupled multilevel cascaded series var compensators', *IEEE Transactions on Industry Applications,* 1998, vol. 34, no. 5, pp. 1156-1163

[8]Choi, S.S., Li, B.H., and Vilathgamuwa, D.M.: 'Design and analysis of the inverter-side filter used in the Dynamic Voltage Restorer', *IEEE Transactions on Power Delivery,* 2002, vol. 17, no. 3, pp. 857-864

[9]Galarza, J.: 'Control of a single-converter voltage-sag and outage compensator', Ph. Thesis, University of Mondragon, Spain, (in Spanish), 2006

[8]Zhang, Y.H., Vilathgamuwa, D.M., and Choi, S.S.: 'An Experimental Investigation of Dynamic Voltage Restorer (DVR)', *IEEE Power Engineering Society Winter Meeting,* Singapore, 2000, pp. 2745-2750

[9]Mihalache, L.: 'DSP control method of single-phase inverters for UPS applications', *IEEE Applied Power Electronics Conference and Exposition, APEC,* Dallas, USA 2002, vol. 1, pp. 590-596

[10]Buso, S., Fasolo, S., and Mattavelli, P.: 'Uninterruptible power supply multiloop control employing digital predictive voltage and current regulators', *IEEE Transactions on Industry Applications,* 2001, vol. 37, no. 6, pp. 1846-1854

[11]Kükrer, O.: 'Deadbeat control of a three-phase inverter with an output LC filter', *IEEE Transactions on Power Electronics,* 1996, vol. 11, no. 1, pp. 16-23

[12]Zhan, C., Ramachandaramurthy, V.K., Arulampalam, A., Fitzer, C., Kromlidis, S., Barnes, M., and Jenkins, N.: 'Dynamic voltage restorer based on voltage-space-vector PWM control', *IEEE Transactions on Industry Applications,* 2001, vol. 37, no. 6, pp. 1855-1863

[13]Kazmierkowski, M.P. and Malesani, L.: 'Current Control Techniques for Three-Phase Voltage-Source PWM Converters: A Survey', *IEEE Transactions on Industrial Electronics,* 1998, vol. 45, no. 5, pp. 691-703

[14]Brando, G., Dannier, A., and Pizzo, A.D.: 'Optimized Predictive Control of a Three-Level NPC PWM-Voltage Source Rectifier', *International Conference on Power Electronics and Intelligent Control for Energy Conservation, PELINCEC,* Warsaw, Poland 2005, Paper ID: 48

[15]Chen, S. and Joós, G.: 'Direct power control of active filters with averaged switching frequency regulation', *IEEE Power Electronics Specialists Conference, PESC,* Aachen, Germany, 2004, pp. 1187-1194,

[16]G.W. Moon: 'Predictive current control of distribution static compensator for reactive power compensation', *IEE Proceedings on Generation, Transmisison and Distribution,* 1999, vol. 146, no. 5, pp. 515-520

[17]Kömürcügil, H. and Kükrer, O.: 'A novel current-control method for three-phase PWM AC/DC voltage-source converters', *IEEE Transactions on Industrial Electronics,* 1999, vol. 46, no. 3, pp. 544-553

[18]Aurtenechea, S., Rodríguez, M. Á., Oyarbide, E., Torrealday, J. R.: 'Predictive Direct Power Control-A New Control Strategy for DC/AC Converters', *32nd Annual Conference of the IEEE Industrial Electronics Society, IECON-2006,* Paris, France, November 2006

[19]Awad, H.: 'Control of static series compensator for mitigation of power quality problems'. Ph. Thesis, Chalmers University, ISBN: 91-7291-406-8, 2004

[20]Svensson, J.: 'Shunt Active Filtering of Vector-current Controlled VSC at a Moderate Switching-frequency', Industry Applications Conference, 1998, 33th IAS Annual Meeting, St. Louis, Missouri, USA, Volume 2, 1998, pp. 1462-1468

[21]Alali, E.: 'Contribution à l'Etude des Compensateurs Actifs des Réseaux Electriques Base Tension', Ph. Thesis, Université Louis Pasteur-Strasbourg I, Strasbourg, 2002

[22]Etxeberria, J.: 'Sur les systèmes d'électronique de puissance dédiés a la distribution électrique- Application a la qualité de l'énergie', Ph. Thesis, Institut National Polytechnique de Grenoble, France, Sept. 2003

10. Appendix

10.1 Derivation of the accuracy of the approximate prediction

In a Taylor series, the accuracy of the n^{th} development-order is bounded by the $(n+1)^{th}$ term. As it can be observed in (8) and (9), the sine development contains only odd terms, while the cosine approximation is built by even terms. Therefore, the maximum approximation error of the sine and cosine Taylor series are:

Even degree of approximation

$$\left|\varepsilon_{\sin}\right|_n < \frac{(\omega_o t)^{n+1}}{(n+1)!} \qquad \left|\varepsilon_{\cos}\right|_n < \frac{(\omega_o t)^{n+2}}{(n+2)!} \tag{28}$$

Odd degree of approximation

$$\left|\varepsilon_{\sin}\right|_n < \frac{(\omega_o t)^{n+2}}{(n+2)!} \qquad \left|\varepsilon_{\cos}\right|_n < \frac{(\omega_o t)^{n+1}}{(n+1)!} \tag{29}$$

Equations (2) and (3) can be organized as:

$$\begin{bmatrix} i_f \\ v_c \end{bmatrix} = \begin{bmatrix} \cos(\omega_0 t) & -C_f\omega_0 \sin(\omega_0 t) \\ L_f\omega_0 \sin(\omega_0 t) & \cos(\omega_0 t) \end{bmatrix} \begin{bmatrix} \Delta i \\ \Delta v \end{bmatrix} + \begin{bmatrix} i_{L0} \\ E \end{bmatrix} \tag{30}$$

with $\Delta i = i_{f0} - i_{L0}$ and $\Delta v = v_{c0} - E$, where i_{L0}, i_{f0}, and v_{c0} are the initial values at the beginning of the state evolution. Combining Eqs (28) and (29) with (30), it is possible to get the prediction error of odd and even approximation orders.

Even degree of approximation

$$\begin{bmatrix} \left|\varepsilon_{if}\right| \\ \left|\varepsilon_{vc}\right| \end{bmatrix} < \begin{bmatrix} \dfrac{(\omega_o t)^{n+2}}{(n+2)!} & C_f\omega_0 \dfrac{(\omega_o t)^{n+1}}{(n+1)!} \\ L_f\omega_0 \dfrac{(\omega_o t)^{n+1}}{(n+1)!} & \dfrac{(\omega_o t)^{n+2}}{(n+2)!} \end{bmatrix} \begin{bmatrix} \left|\Delta i\right| \\ \left|\Delta v\right| \end{bmatrix} \tag{31}$$

Odd degree of approximation

$$\begin{bmatrix} \left|\varepsilon_{if}\right| \\ \left|\varepsilon_{vc}\right| \end{bmatrix} < \begin{bmatrix} \dfrac{(\omega_o t)^{n+1}}{(n+1)!} & C_f\omega_0 \dfrac{(\omega_o t)^{n+2}}{(n+2)!} \\ L_f\omega_0 \dfrac{(\omega_o t)^{n+2}}{(n+2)!} & \dfrac{(\omega_o t)^{n+1}}{(n+1)!} \end{bmatrix} \begin{bmatrix} \left|\Delta i\right| \\ \left|\Delta v\right| \end{bmatrix} \tag{32}$$

Supposing an application time of half the switching period, $t = T_{sw}/2$, and considering the relation (12), the following equation can be derived directly:

$$\omega_0 t = \frac{\pi}{m} \tag{33}$$

The following equation can also be derived directly:

$$C_f\omega_0 = \sqrt{\frac{C_f}{L_f}} \qquad L_f\omega_0 = \sqrt{\frac{L_f}{C_f}} \tag{34}$$

Combining (33) and (34) with (31) and (32) it is possible to get the prediction-accuracy values as a function of the development order *n* and the frequency ratio *m*.

Even degree of approximation

$$\begin{bmatrix} \left|\varepsilon_{if}\right| \\ \left|\varepsilon_{vc}\right| \end{bmatrix} < \begin{bmatrix} \dfrac{\pi^{n+2}}{m^{n+2}(n+2)!} & \sqrt{\dfrac{C_f}{L_f}}\dfrac{\pi^{n+1}}{m^{n+1}(n+1)!} \\ \sqrt{\dfrac{L_f}{C_f}}\dfrac{\pi^{n+1}}{m^{n+1}(n+1)!} & \dfrac{\pi^{n+2}}{m^{n+2}(n+2)!} \end{bmatrix} \begin{bmatrix} \left|\Delta i\right| \\ \left|\Delta v\right| \end{bmatrix} \tag{35}$$

Odd degree of approximation

$$\begin{bmatrix} \left|\varepsilon_{if}\right| \\ \left|\varepsilon_{vc}\right| \end{bmatrix} < \begin{bmatrix} \dfrac{\pi^{n+1}}{m^{n+1}(n+1)!} & \sqrt{\dfrac{C_f}{L_f}}\dfrac{\pi^{n+2}}{m^{n+2}(n+2)!} \\ \sqrt{\dfrac{L_f}{C_f}}\dfrac{\pi^{n+2}}{m^{n+2}(n+2)!} & \dfrac{\pi^{n+1}}{m^{n+1}(n+1)!} \end{bmatrix} \begin{bmatrix} \left|\Delta i\right| \\ \left|\Delta v\right| \end{bmatrix} \tag{36}$$

This leads directly to Eqs (10) and (11).

10.2 Derivation of the application times

The SO-PDC problem leads to the next set of seven equations and seven variables:

$$t_3 = T_{sw} - t_1 - t_2 \tag{37}$$

$$i_{f1} \approx \frac{E_1 - v_{c0}}{L_f} t_1 + i_{f0}\left(1 - \frac{\omega_o^2 t_1^2}{2}\right) + i_{L0}\frac{\omega_o^2 t_1^2}{2} \tag{38}$$

$$v_{c1} \approx v_{c0}\left(1 - \frac{\omega_o^2 t_1^2}{2}\right) + E_1\frac{\omega_o^2 t_1^2}{2} + i_{f0}L_f\omega_o^2 t_1 - i_{L0}L_f\omega_o^2 t_1 \tag{39}$$

$$i_{f2} \approx \frac{E_2 - v_{c1}}{L_f} t_2 + i_{f1}\left(1 - \frac{\omega_o^2 t_2^2}{2}\right) + i_{L0}\frac{\omega_o^2 t_2^2}{2} \tag{40}$$

$$v_{c2} \approx v_{c1}\left(1 - \frac{\omega_o^2 t_2^2}{2}\right) + E_2\frac{\omega_o^2 t_2^2}{2} + i_{f1}L_f\omega_o^2 t_2 - i_{L0}L_f\omega_o^2 t_2 \tag{41}$$

$$i_{f3} \approx \frac{E_3 - v_{c2}}{L_f} t_2 + i_{f2}\left(1 - \frac{\omega_o^2 t_3^2}{2}\right) + i_{L0}\frac{\omega_o^2 t_3^2}{2} \tag{42}$$

$$v_{c3} \approx v_{c2}\left(1 - \frac{\omega_o^2 t_3^2}{2}\right) + E_3\frac{\omega_o^2 t_3^2}{2} + i_{f2}L_f\omega_o^2 t_3 - i_{L0}L_f\omega_o^2 t_3 \tag{43}$$

Replacing i_{f1} and v_{c1} in (40) and (41) by (38) and (39), inserting the resulting i_{f2} and v_{c2} expressions in (42) and (43), and considering (37), a set of two equations (44) and (45) and two variables (t_1, t_2) is obtained.

$$i_{f3} = f_1(T_{sw}, t_1, t_2, i_{f0}, v_{c0}, i_{L0}, E_1, E_2, E_3) \tag{44}$$

$$v_{c3} = f_2(T_{sw}, t_1, t_2, i_{f0}, v_{c0}, i_{f3}, i_{L0}, E_1, E_2, E_3) \tag{45}$$

Considering only the terms of order two or lower, the next equation can be derived from (44):

$$t_1 = \frac{1}{c_0}\left(c_1 t_2 + c_2 i_{f3} + (c_3 - c_2) i_{f0} + c_4 v_{c0} - c_3 i_{L0} - c_5\right) \qquad (46)$$

with

$$c_0 = E_1 - E_3$$
$$c_1 = E_3 - E_2$$
$$c_2 = L_f$$
$$c_3 = \frac{\omega_0^{\,2} T_{sw}^{\,2} L_f}{2}$$
$$c_4 = T_{sw}$$
$$c_5 = c_4 E_3$$

Replacing (46) in (45) and considering only the terms of order two or lower, the next simple second-order equation is obtained:

$$\frac{a_0 \omega_0}{2} t_2^{\,2} - \frac{2 b_0}{a_0 \omega_0} = 0 \qquad (47)$$

with

$$\begin{aligned} b_0 = {} & -a_1 a_2 v_{c3} - a_3 i_{f3}^{\,2} - a_4 v_{c0} i_{f3} - a_5 i_{f0} i_{f3} + a_6 i_{L0} i_{f3} + \\ & + a_7 i_{f3} + a_8 v_{c0}^{\,2} + a_9 v_{c0} i_{f0} + a_{10} i_{L0} v_{c0} + a_{11} v_{c0} + \\ & + a_{12} i_{f0}^{\,2} + a_{13} i_{L0} i_{f0} + a_{14} i_{f0} + a_{15} i_{L0}^{\,2} + a_{16} i_{L0} + a_{17} \end{aligned}$$
$$a_0 = 4E_1E_3 - 4E_2E_3 - 4E_1E_2 + 4E_2^{\,2}$$
$$a_1 = -E_1E_3 + E_1E_2 - E_2^{\,2} + E_3E_2$$
$$a_2 = 8(E_1 - E_3)$$
$$a_3 = -4a_1\omega_0^{\,2}L_f^{\,2}$$
$$a_4 = 2T_{sw}a_3$$
$$a_5 = a_3\left(\omega_0^{\,2}T_{sw}^{\,2} - 2\right)$$
$$a_6 = 4a_1\omega_0^{\,4}L_f^{\,2}T_{sw}^{\,2}$$
$$a_7 = 8a_1E_1\omega_0^{\,2}L_fT_{sw}$$
$$a_8 = -4a_1\omega_0^{\,2}T_{sw}^{\,2}$$
$$a_9 = \frac{a_5T_{sw}}{L_f}$$
$$a_{10} = 4a_1\omega_0^{\,4}L_fT_{sw}^{\,3}$$
$$a_{11} = -4a_1\left(2E_3 - E_1\omega_0^{\,2}T_{sw}^{\,2} - \omega_0^{\,2}T_{sw}^{\,2}E_3 - 2E_1\right)$$
$$a_{12} = -a_1\omega_0^{\,2}L_f^{\,2}\left(\omega_0^{\,4}T_{sw}^{\,4} - 4\omega_0^{\,2}T_{sw}^{\,2} + 4\right)$$
$$a_{13} = -2a_1\omega_0^{\,4}L_f^{\,2}T_{sw}^{\,2}\left(-\omega_0^{\,2}T_{sw}^{\,2} + 2\right)$$
$$a_{15} = -a_1\omega_0^{\,6}T_{sw}^{\,4}L_f^{\,2}$$
$$a_{16} = -4a_1\omega_0^{\,2}L_fT_{sw}\left(E_1\omega_0^{\,2}T_{sw}^{\,2} + 2E_1 - 2E_3\right)$$
$$a_{17} = -4a_1E_1\omega_0^{\,2}T_{sw}^{\,2}E_3$$

By solving (47), the following equation is obtained directly:

$$t_2 = \frac{\pm 2\sqrt{b_0}}{a_0\omega_0} \qquad (48)$$